minerals

MDPI

Article

Equation of State of a Natural Chromian Spinel at Ambient Temperature

Zhongying Mi [1,2,3], Weiguang Shi [4], Lifei Zhang [1,2], Sean R. Shieh [3] and Xi Liu [1,2,*]

1 School of Earth and Space Sciences, Peking University, Beijing 100871, China; zhongying.mi@pku.edu.cn (Z.M.); lfzhang@pku.edu.cn (L.Z.)
2 Key Laboratory of Orogenic Belts and Crustal Evolution, Ministry of Education of China, Beijing 100871, China
3 Department of Earth Sciences, University of Western Ontario, London, ON N6A 5B7, Canada; sshieh@uwo.ca
4 College of Chemistry & Chemical Engineering, Northeast Petroleum University, Daqing 163318, China; sswwgg2004@gmail.com
* Correspondence: xi.liu@pku.edu.cn; Tel.: +86-10-62753585

Received: 13 November 2018; Accepted: 5 December 2018; Published: 13 December 2018

Abstract: A natural chromian spinel with the composition $(Mg_{0.48(3)}Fe_{0.52(3)})(Fe_{0.06(1)}Al_{0.28(1)}Cr_{0.66(2)})_2O_4$ was investigated up to 15 GPa via synchrotron X-ray diffraction with a diamond-anvil cell at room temperature. No phase transition was clearly observed up to the maximum experimental pressure. The pressure–volume data fitted to the third-order Birch–Murnaghan equation of state yielded an isothermal bulk modulus (K_{T0}) of 207(5) GPa and its first pressure derivative (K'_{T0}) of 3.2(7), or K_{T0} = 202(2) GPa with K'_{T0} fixed as 4. With this new experimental result and the results on some natural chromian spinels in the literature, a simple algorithm describing the relation between the K_{T0} and the compositions of the natural chromian spinels was proposed. To examine this algorithm further, more compression experiments should be performed on natural chromian spinels with different chemical compositions.

Keywords: chemical composition; diamond anvil-cell; equation of state; natural chromian spinel

1. Introduction

The 2-3 spinel oxides, with the general chemical formula AB_2O_4 (A = 2+ and B = 3+), as well as the so-called 4-2 spinel oxides (A = 4+ and B = 2+; ringwoodite $(Mg,Fe)_2SiO_4$-spinel for example), are geologically important minerals, and are frequently found in different types of rocks in different geological settings [1]. They all have the cubic $Fd\bar{3}m$ structure, but show wide compositional variation [2]. Due to their compositional diversity, they have been used as key petrogenetic indicators of many geological processes [2–4] and played important roles in constraining pressure, temperature, oxygen fugacity, and other quantities [5–7].

The only major mineral source for metal chromium is the 2-3 natural chromian spinels (termed as Sp_{ss} hereafter) [8]. These chromian spinels are also among the most common mineral inclusions found in cratonic diamonds, and therefore can be used to estimate the formation P and T of the diamonds. To achieve this goal of the P–T estimation, the isothermal bulk moduli (K_{T0}) of the natural chromian spinels and their compositional dependence should be accurately known. To date, there have been very limited experimental studies on the K_{T0} of the Sp_{ss} [9–11]. Considering the complicated correlations between the K_{T0} and compositions of the solid solution series of some minerals [12–14], more experimental investigations should be conducted to determine the K_{T0} of the Sp_{ss} with different compositions.

In this study, the K_{T0} of an Sp_{ss} was determined by performing compression experiments at room T using a diamond-anvil cell (DAC) coupled with synchrotron X-ray radiation. Comparing this new result with the results in the literature, the correlation between the K_{T0} and the compositions of the Sp_{ss} is tentatively discussed.

2. Experimental Method

The Sp_{ss}-bearing sample was sourced from the Big Daddy Deposit, Sudbury, ON, Canada [15]. The spinel crystals were black and exhibited good octahedral shape (grain size up to ~400 μm). Nineteen electron microprobe analyses were done with a JEOL JXA-8100 at the School of Earth and Space Sciences, Peking University and gave out the following compositional data, FeO 23.20 wt %, MgO 10.04 wt %, Cr_2O_3 51.49 wt %, and Al_2O_3 14.86 wt %, leading to the chemical formula of $(Mg_{0.48(3)}Fe_{0.52(3)})(Fe_{0.06(1)}Al_{0.28(1)}Cr_{0.66(2)})_2O_4$. Some spinel crystals were picked up and ground into a fine powder, which was then loaded into a DAC. In the DAC experiments, we used a rhenium gasket and a Neon pressure medium, which was loaded by employing the GSECARS high-pressure gas- loading system. A flake of gold (~20 μm in diameter) was placed on the top of the sample to serve as pressure standard and position marker. In-situ high-pressure synchrotron X-ray diffraction experiments with the loaded DAC were performed up to ~15.00 GPa at the beamline 16-ID-B of HPCAT, the Advanced Photon Source of the Argonne National Laboratory. The sample was probed with a monochromatic X-ray beam (beam size 3 × 3 μm^2, wavelength 0.37379 Å) and the data were collected with a 2-dimensional CCD detector. The sample-to-detector distance and orientation of the detector were calibrated by using a CeO_2 powder standard.

3. Result and Discussion

In total, 26 X-ray diffraction (XRD) patterns were collected at pressures from 0.90 to 15.00 GPa (Table 1), with the pressures determined using the Au equation of state (EoS) from Fei et al. [16]. Some XRD patterns are shown in Figure 1. As pressure increases, all XRD peaks shift continuously toward higher 2θ angles. No apparent peak-splitting or new peak has been observed, indicating no phase transition for this spinel up to the maximum experimental pressure. However, several XRD peaks such as the 311 and 511 peaks show slight peak-broadening, potentially implying a structural instability which was somehow kinetically hindered due to the low experimental temperature. The used pressure medium neon can maintain a good hydrostatic experimental condition up to ~15 GPa [17], and should not be the major reason for the observed minor peak-broadening. To ensure a high accuracy in the unit-cell volume refinement, we excluded the peaks 311 and 511 because of their slight broadening.

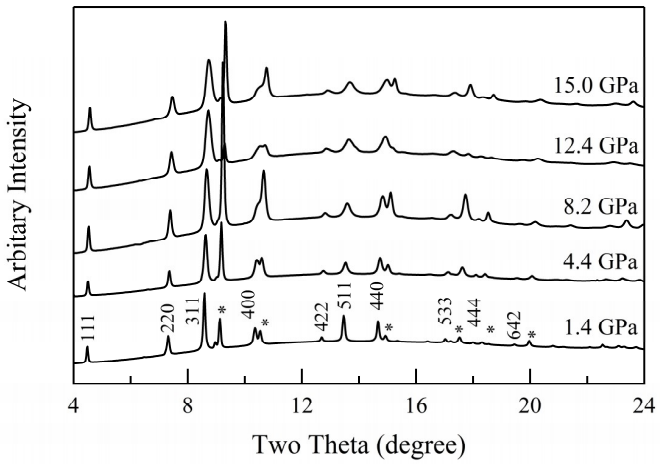

Figure 1. Some X-ray diffraction patterns of the natural chromian spinel (cubic $Fd\bar{3}m$) at 1.4, 4.4, 8.2, 12.4, and 15.0 GPa. All major peaks can be assigned to the structures of our 2-3 natural chromian spinels (Sp_{ss}) and Au (marked with asterisks).

Table 1. Unit-cell parameters of chromium spinel at high pressures.

P (GPa)	*a* (Å)	*V* (Å^3)
0.90(7) [a]	8.284(1)	568.57(14)
1.37(1)	8.281(1)	567.76(11)
1.46(2)	8.283(2)	567.76(38)
1.78(3)	8.275(2)	566.70(38)
2.07(1)	8.270(1)	565.59(26)
2.17(2)	8.270(1)	565.53(27)
3.06(1)	8.258(1)	563.10(25)
3.61(6)	8.249(1)	561.21(24)
4.46(4)	8.240(1)	559.45(22)
5.87(5)	8.223(2)	556.08(30)
6.92(6)	8.213(1)	553.97(19)
8.24(4)	8.196(2)	550.49(35)
9.36(2)	8.181(2)	547.58(46)
10.20(2)	8.172(3)	545.74(52)
10.96(9)	8.163(3)	543.89(52)
11.45(7)	8.159(2)	543.03(48)
12.37(1)	8.150(2)	541.25(46)
12.39(6)	8.147(2)	540.80(33)
12.42(8)	8.145(4)	540.26(69)
12.86(7)	8.139(3)	539.11(63)
13.10(8)	8.135(3)	538.44(59)
13.33(9)	8.133(3)	537.99(59)
13.62(10)	8.130(3)	537.43(67)
13.93(5)	8.124(4)	536.22(87)
14.46(4)	8.123(4)	535.89(74)
15.00(4)	8.117(3)	534.84(66)

[a] Numbers in parentheses represent one standard deviation.

The *P*–*V* data are summarized in Table 1 and shown in Figure 2. They were fitted to the third-order Birch–Murnaghan equation of state (BM-EoS; [18]):

$$P = \frac{3}{2}K_{T0}\left[\left(\frac{V_0}{V}\right)^{\frac{7}{3}} - \left(\frac{V_0}{V}\right)^{\frac{5}{3}}\right]\left\{1 + \frac{3}{4}\left(K'_{T0} - 4\right)\left[\left(\frac{V_0}{V}\right)^{\frac{2}{3}} - 1\right]\right\}, \quad (1)$$

where P is the pressure (GPa), K_{T0} the isothermal bulk modulus (GPa), K'_{T0} the first pressure derivative of the K_{T0}, V_0 the volume at zero pressure, and V the volume at high pressure. Using the software EosFit 5.2 [19], we obtained K_{T0} = 207(5) GPa, K'_{T0} = 3.2(7), and V_0 = 571.69(15) Å^3, or K_{T0} = 202(2) GPa with K'_{T0} fixed to 4 and V_0 = 571.79(10) Å^3.

The quality of our derived BM-EoS can be evaluated by a linear fitting of the normalized pressure (F) as a function of the Eulerian strain (f_E) (i.e., the f_E–F plot) [20]. The two variables, F and f_E, are defined as:

$$F = \frac{P}{3f_E(1 + 2f_E)^{\frac{5}{2}}} \quad (2)$$

and

$$f_E = \frac{1}{2}\left[\left(\frac{V_0}{V}\right)^{\frac{2}{3}} - 1\right]. \quad (3)$$

The third-order BM-EoS can then be rewritten as:

$$F = \frac{3}{2}K_{T0}\left(K'_{T0} - 4\right)f_E + K_{T0}, \quad (4)$$

where the slope of the line defined by the experimental data is equal to $3/2K_{T0}(K'_{T0} - 4)$, and the intercept value is the K_{T0}. Accordingly, a slope of zero means K'_{T0} = 4, a negative slope K'_{T0} < 4, and a

positive slope $K'_{T0} > 4$. Figure 3 clearly shows that the K'_{T0} of our Sp_{ss} should be close to 4, supporting a 2nd-order truncation of the BM-EoS fit.

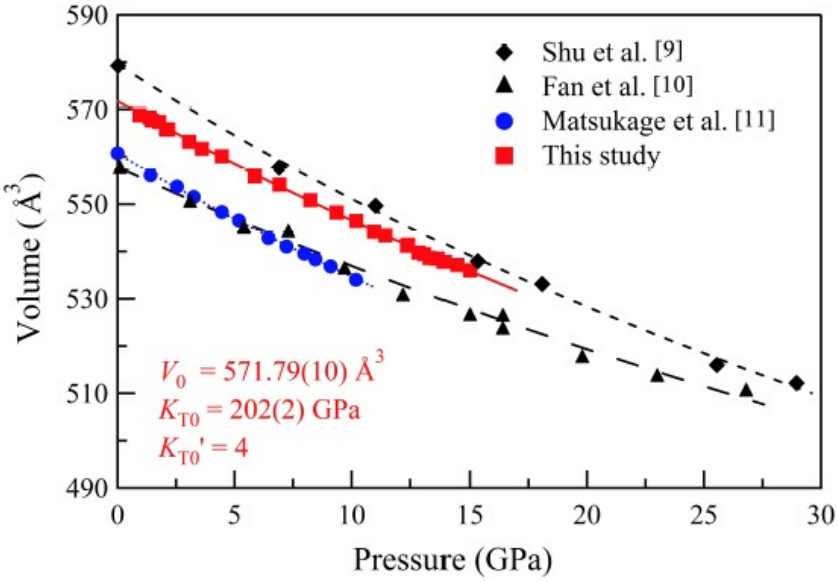

Figure 2. Effect of pressure on the volume of some Sp_{ss} (300 K). Note that most experimental data points have error bars approximate to or smaller than the symbols. Shu et al. [9], $(Mn_{0.02}Mg_{0.30}Fe_{0.68})(Al_{0.07}Fe_{0.10}Cr_{0.83})_2O_4$; Fan et al. [10], $(Na_{0.01}Mg_{0.68}Fe_{0.28})_{0.97}(Cr_{1.49}Al_{0.54})_{2.03}O_4$; Matsukage et al. [11], $(Mg_{0.77}Fe_{0.23})(Cr_{0.46}Al_{0.5}Fe_{0.04})_2O_4$. The curves are drawn using the second-order Birch–Murnaghan equation of state, as listed in Table 2. The equations in red are for the natural chromian spinel, $(Mg_{0.48}Fe_{0.52})(Fe_{0.06}Al_{0.28}Cr_{0.66})_2O_4$, investigated in this study.

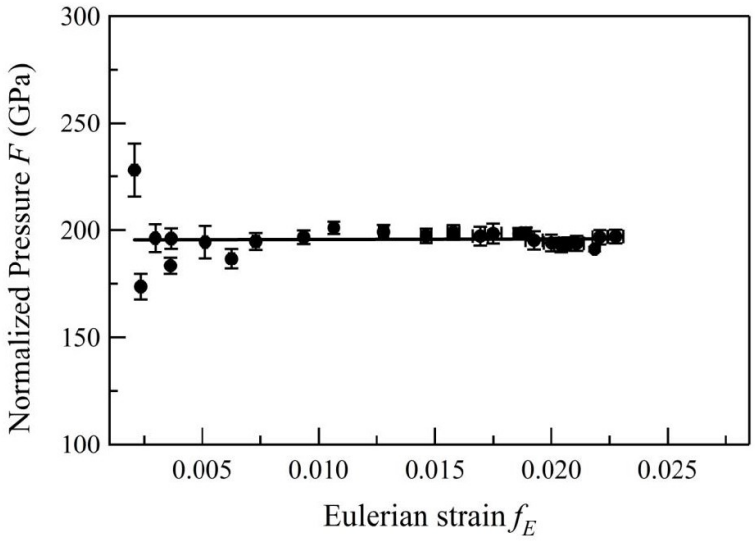

Figure 3. Eulerian strain-normalized pressure (f_E–F) plot. Standard deviations were calculated following the method from Heinz and Jeanloz [21]. The solid line represents a weighted linear fit through our data.

Following Matsukage et al. [11], our Sp_{ss} can be viewed as a complicated solid solution made of the following six end-members, spinel (Sp, $MgAl_2O_4$), hercynite (He, $FeAl_2O_4$), magnesiochromite (Mg-Ch, $MgCr_2O_4$), chromite (Ch, $FeCr_2O_4$), magnesioferrite (Mg-Fe, $MgFe_2O_4$), and magnetite (Ma, Fe_3O_4), with their mole percentages calculated as 13.44%, 14.56%, 31.68%, 34.32%, 2.88%, and 3.12%, respectively. The K_{T0} values of these six end-members were experimentally constrained, and are summarized in Table 2. On the assumption of K'_{T0} = 4 for all spinel oxides, as proposed by

Liu et al. [13,14], the K_{T0} of our Sp_{ss} ($Sp_{13}He_{15}Mg\text{-}Ch_{32}Ch_{34}Mg\text{-}Fe_3Ma_3$) was approximated as 193.4(7) GPa with the following simple algorithm:

$$K_{T0-Sp_{ss}} = \sum x_i K_{T0-i}, \quad (5)$$

where $K_{T0-Sp_{ss}}$ denotes the K_{T0} of the Sp_{ss}, x_i the mole fraction of the i-th end-member, and K_{T0-i} the K_{T0} of the i-th end-member. The absolute difference and relative difference between the approximated bulk modulus and our experimentally measured value were only ~9 GPa and ~4.5%, respectively.

Table 2. Birch–Murnaghan equation of state (BM-EoS) parameters of some Sp_{ss}, and their six end-members (ambient P and T).

Spinel	V_0	K_{T0}	K'_{T0}	Experimental Details [a]	Reference
Sp_{ss}	571.7(1) [b]	207(5)	3.2(7)	0–15; Gold; Ne; Powder	This study
	571.8(1)	202(2)	4		
Sp_{ss}	579.6(9)	179(10)	3.9(9)	0–29; Ruby; He; SC	[9]
	579.6(9)	179(1)	4 [c]		
Sp_{ss}	557.86	209(9)	7(1)	0–26.8; Mo; MEW; Powder	[10]
	556.5(8)	242(7)	4 [c]		
Sp_{ss}	560.6(2)	192(7)	4(1)	0–10.19; Ruby; ME; Powder	[11]
	560.6(2)	192(7)	3.6(13)		
$MgAl_2O_4$	529.37	196(1)	4.7(3)	0–65; Gold; ME; powder	[22]
Sp		529.37	201.6(6)	4 [c]	
$FeAl_2O_4$	542.58	193.9(2)	6.0(5)	0–7.5; Quartz; ME; SC	[23]
He		542.58	200.9(7)	4 [c]	
$MgCr_2O_4$	573.9	182.5(4)	5.8(4)	0–8.2; Quartz; ME; SC	[24]
Mg-Ch	573.9	189.6(7)	4 [c]		
$FeCr_2O_4$	588.47	184.8(2)	6.1(5)	0–9.2; Quartz; ME; SC	[24]
Ch		588.47	193(1)	4 [c]	
$MgFe_2O_4$	590.7	179(2)	3.3(2)	0–53; Ruby; He; Powder	[25]
Mg-Fe	590.7	170.5(8)	4 [c]		
Fe_3O_4	591.5	181(2)	5.5(15)	0–4.5; Ruby; ME; SC	[26]
Ma	591.5	187(11)	4 [c]		

[a] All compression experiments were done with the diamond-anvil cell (DAC), with some of the experimental details listed in the following order: P range (GPa), pressure scale, pressure medium, and XRD method. Gold, pressure scale of gold from Fei et al. [16] or Heinz and Jeanloz [21]; Ruby, pressure scale of ruby from Mao et al. [27]; Mo, pressure scale of Zhao et al. [28]; Quartz, pressure scale of quartz from Angel et al. [29]. Ne, pressure medium of neon; He, pressure medium of helium; MEW, pressure medium of a 16:3:1 methanol–ethanol–water mixture; ME, pressure medium of a 4:1 methanol–ethanol mixture. Powder, powder XRD; SC, single-crystal XRD. [b] Numbers in parentheses represent one standard deviation. [c] If the reference did not provide the value of K_{T0} at K'_{T0} = 4, we calculated it from the P–V data.

Matsukage et al. [11] compressed another Sp_{ss} ($Sp_{38}He_{12}Mg\text{-}Ch_{35}Ch_{11}Mg\text{-}Fe_3Ma_1$) with the chemical formula $(Mg_{0.77}Fe_{0.23})(Cr_{0.46}Al_{0.5}Fe_{0.04})_2O_4$ using similar experimental techniques (Table 2; Figure 2). The experimentally-obtained K_{T0} was 192 GPa, and the approximated K_{T0} with the above algorithm was 195 GPa, suggesting a relative difference of only 1.5%. Shu et al. [9] studied another Sp_{ss} ($Sp_2He_5Mg\text{-}Ch_{25}Ch_{56}Mg\text{-}Fe_3Ma_7Mn_2$; Mn standing for manganochromite, $MnCr_2O_4$) with the chemical formula $(Mn_{0.02}Mg_{0.30}Fe_{0.68})(Al_{0.07}Fe_{0.10}Cr_{0.83})_2O_4$. The experimentally-obtained K_{T0} was 179 GPa (Table 2) and the approximated K_{T0} was 193 GPa, suggesting a large relative difference of 8%, which was presumably caused by the limited and scattering data points (seven data as shown in Figure 2). Fan et al. [10] investigated another Sp_{ss} ($Sp_{19}He_8Mg\text{-}Ch_{51}Ch_{22}$) with the chemical formula $(Na_{0.01}Mg_{0.68}Fe_{0.28})_{0.97}(Cr_{1.49}Al_{0.54})_{2.03}O_4$ (Figure 2). Fitting their P–V data at room T to Equation (1), we obtained K_{T0} = 242(7) GPa as K'_{T0} fixed at 4 or K_{T0} = 194(17) GPa with K'_{T0} = 9(2). In comparison, the approximated K_{T0} was only 192 GPa, being 50 GPa smaller than the experimentally-obtained value (with a large relative difference of ~21%; K'_{T0} fixed at 4). As pointed out by Fan et al. [10], the 16:3:1

methanol–ethanol–water mixture pressure medium used in their experiments resulted in somewhat non-hydrostatic experimental condition at P > ~10 GPa, which in turn should have led to the nominally much larger K_{T0} [30].

It is rather interesting that the simple algorithm of Equation (5) could reproduce so well the K_{T0} values of the Sp_{ss} established by the properly-performed experiments, but reject the K_{T0} values of the Sp_{ss} yielded by the malfunctioned experiments (Figure 4); According to our experience, a relative difference of ~5% (or even much larger) among the K_{T0} values determined for certain minerals using similar experimental techniques is not unusual [7,13]. If this observation is confirmed by further experimental studies on the Sp_{ss} of different compositions, Equation (5) may provide a convenient method to estimate the K_{T0} of those Sp_{ss} inclusions hosted by the diamonds. Meanwhile, we should keep in mind that Liu et al. [14] discovered a non-monotonic correlation between the K_{T0} and composition for the $(Mg_{1-x}Mn_x)Cr_2O_4$ spinel solid solutions. Nevertheless, it is highly possible that the cations in the Sp_{ss} might more randomly enter the spinel structure, which should then result in a generally ideal mixing behavior, whereas the Mg and Mn cations in the $(Mg_{1-x}Mn_x)Cr_2O_4$ spinel solid solutions can compete for the T-site only, which eventually leads to a significant deviation from an ideal mixing.

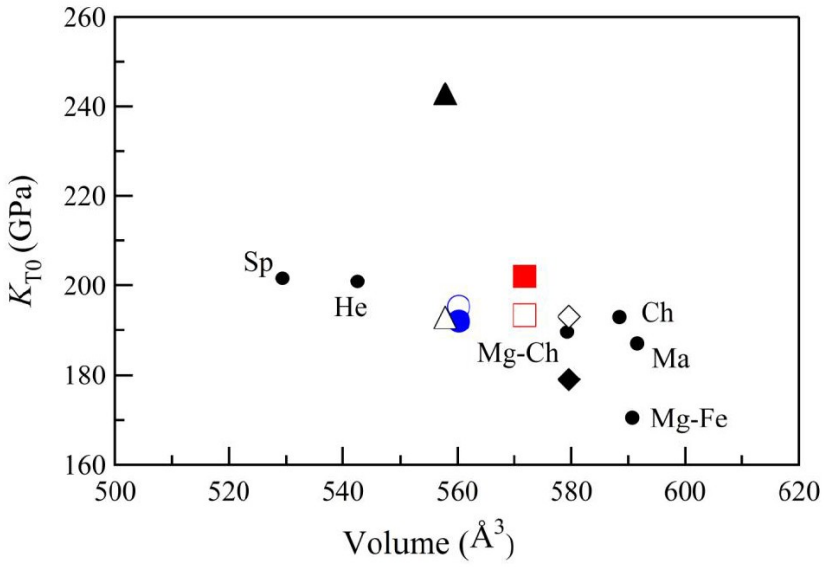

Figure 4. K_{T0} vs. V_0 of some Sp_{ss} and their six end-members Sp, He, Mg-Ch, Ch, Ma, and Mg-Fe. The plotted experimental results and their sources for the six end-members, plus some experimental details, are listed in Table 2. The symbols for the Sp_{ss} are the same as those in Figure 2, with the filled symbols standing for the experimental results whereas the empty symbols represent the approximated results. Note that the Sp_{ss} from [9] can be recasted as $Sp_2He_5Mg\text{-}Ch_{25}Ch_{56}Mg\text{-}Fe_3Ma_7Mn_2$; that from [10] as $Sp_{19}He_8Mg\text{-}Ch_{51}Ch_{22}$; that from [11] as $Sp_{38}He_{12}Mg\text{-}Ch_{35}Ch_{11}Mg\text{-}Fe_3Ma_1$; and that from this study as $Sp_{13}He_{15}Mg\text{-}Ch_{32}Ch_{34}Mg\text{-}Fe_3Ma_3$. The Sp_{ss} from [9] has 2% manganochromite (Mn, $MnCr_2O_4$), which has K_{T0} = 199.2(106) GPa with a fixed K'_{T0} of 4 [14].

Author Contributions: Conceptualization, X.L. and S.R.S.; Validation, X.L.; Investigation, Z.M., W.S.; Writing—Original Draft Preparation, Z.M.; Writing—Review & Editing, X.L.; Supervision, X.L., S.R.S., L.Z.; Project Administration, X.L.; Funding Acquisition, X.L., S.R.S., L.Z. All authors discussed the results and commented on the manuscript.

Funding: This research is financially supported by the Strategic Priority Research Program (B) of CAS (XDB18000000), the National Natural Science Foundation of China (#11404362), the Shanghai Sailing Plan (14YF1407400), and by the NSERC.

Acknowledgments: The authors thank Norman Duke for providing samples. We are grateful for the experimental assistance from Stanislav Sinogeikin at HPCAT 16-ID-B, Advanced Photon Source (APS) of Argonne National Laboratory.

Conflicts of Interest: The authors declare no conflict of interests.

References

1. Biagioni, C.; Pasero, M. The systematics of the spinel-type minerals: An overview. *Am. Mineral.* **2014**, *99*, 1254–1264. [CrossRef]
2. Barnes, S.J.; Roeder, P.L. The range of spinel compositions in terrestrial mafic and ultramafic rocks. *J. Petrol.* **2001**, *42*, 2279–2302. [CrossRef]
3. Dick, H.J.B.; Bullen, T. Chromian spinel as a petrogenetic indicator in abyssal and alpine-type peridotites and spatially associated lavas. *Contrib. Mineral. Petr.* **1984**, *86*, 54–76. [CrossRef]
4. Liu, X.; O'Neill, H.St.C. The effect of Cr_2O_3 on the partial melting of spinel lherzolite in the system CaO-MgO-Al_2O_3-SiO_2-Cr_2O_3 at 1.1 GPa. *J. Petrol.* **2004**, *45*, 2261–2286. [CrossRef]
5. O'Neill, H.St.C. The transition between spinel lherzolite and garnet lherzolite, and its use as a geobarometer. *Contrib. Mineral. Petr.* **1981**, *77*, 185–194. [CrossRef]
6. Ballhaus, C.; Berry, R.F.; Green, D.H. Oxygen fugacity controls in the Earth's upper mantle. *Nature* **1990**, *349*, 437–449. [CrossRef]
7. Zhang, Y.; Liu, X.; Xiong, Z.; Zhang, Z. Compressional behavior of $MgCr_2O_4$ spinel from first-principles simulation. *Sci. China-Earth Sci.* **2016**, *59*, 989–996. [CrossRef]
8. Duke, J.M. Ore deposit models 7. magmatic segregation deposits of chromite. *Geosci. Can.* **1983**, *10*, 15–24.
9. Shu, J.F.; Mao, W.L.; Hemley, R.J.; Mao, H.K. Pressure-induced distortive phase transition in chromite-spinel at 29 GPa. *Mater. Res. Soc. Symp. P.* **2007**, *987*, 179–184.
10. Fan, D.W.; Zhou, W.G.; Liu, C.Q.; Liu, Y.G.; Jiang, X.; Wan, F.; Liu, J.; Li, X.D.; Xie, H.S. Thermal equation of state of natural chromium spinel up to 26.8 GPa and 628 K. *J. Mater. Sci.* **2008**, *43*, 5546–5550. [CrossRef]
11. Matsukage, K.N.; Kikuchi, S.; Ono, S.; Nishihara, Y.; Kikegawa, T. Density and seismic velocities of chromitite body in oceanic mantle peridotite. *Am. Mineral.* **2010**, *95*, 1422–1428. [CrossRef]
12. Du, W.; Clark, S.M.; Walker, D. Thermo-compression of pyrope-grossular garnet solid solutions: Non-linear compositional dependence. *Am. Mineral.* **2015**, *100*, 215–222. [CrossRef]
13. Liu, X.; Xiong, Z.; Chang, L.; He, Q.; Wang, F.; Shieh, S.R.; Wu, C.; Li, B. and Zhang, L. Anhydrous ringwoodites in the mantle transition zone: Their bulk modulus, solid solution behavior, compositional variation, and sound velocity feature. *Solid Earth Sci.* **2016**, *1*, 28–47. [CrossRef]
14. Liu, X.; Xiong, Z.; Shieh, S.R.; He, Q.; Deng, L.; Zhang, Y.; Chang, L.; Wang, F.; Hong, X.; Chen, Z. Non-monotonic compositional dependence of isothermal bulk modulus of the $(Mg_{1-x}Mn_x)Cr_2O_4$ spinel solid solutions, and its origin and implication. *Solid Earth Sci.* **2016**, *1*, 89–100. [CrossRef]
15. Aubut, A. National Instrument 43-101Technical Report: Big Daddy chromite deposit, McFaulds Lake Area, Ontario, Canada, Porcupine Mining Division, NTS 43D16. In *Mineral Resource Estimation Technical Report Prepared for KWG Resources Inc. Sibley Basin Group*; 2012; pp. 1–64. Available online: http://www.kwgresources.com/_resources/pdfs/tech_report.pdf (accessed on 9 September 2018).
16. Fei, Y.W.; Ricolleau, A.; Frank, M.; Mibe, K.; Shen, G.Y.; Prakapenka, V. Toward an internally consistent pressure scale. *Proc. Natl. Acad. Sci.* **2007**, *104*, 9182–9186. [CrossRef] [PubMed]
17. Klotz, S.; Chervin, J.C.; Munsch, P.; Lemarchand, G. Hydrostatic limits of 11 pressure transmitting media. *J. Phys. D* **2009**, *42*, 075413. [CrossRef]
18. Birch, F. Finite elastic strain of cubic crystals. *Phys. Rev.* **1947**, *71*, 809–824. [CrossRef]
19. Angel, R.J. Equation of state. *Rev. Mineral. Geochem.* **2000**, *41*, 35–60. [CrossRef]
20. Birch, F. Finite strain isotherm and velocities for single-crystal and polycrystalline NaCl at high pressures and 300°K. *J. Geophys. Res.* **1978**, *83*, 1257–1268. [CrossRef]
21. Heinz, D.L.; Jeanloz, R. The equation of state of the gold calibration standard. *J. Appl. Phys.* **1984**, *55*, 885–893. [CrossRef]
22. Kruger, M.B.; Nguyen, J.H.; Caldwell, W.; Jeanloz, R. Equation of state of $MgAl_2O_4$ spinel to 65 GPa. *Phys. Rev. B* **1997**, *56*, 1–4. [CrossRef]
23. Nestola, F.; Periotto, B.; Anzolini, C.; Andreozzi, G.B.; Woodland, A.B.; Lenaz, D.; Alvaro, M.; Princivalle, F. Equation of state of hercynite, $FeAl_2O_4$, and high-pressure systematics of Mg-Fe-Cr-Al spinels. *Mineral. Mag.* **2015**, *79*, 285–294. [CrossRef]

24. Nestola, F.; Periotto, B.; Andreozzi, G.B.; Bruschini, E.; Bosi, F. Pressure-volume equation of state for chromite and magnesiochromite: A single-crystal X-ray diffraction investigation. *Am. Mineral.* **2014**, *99*, 1248–1253. [CrossRef]
25. Greenberg, E.; Rozenberg, G.Kh.; Xu, W.; Arielly, R.; Pasternak, M.P.; Melchior, A.; Garbarino, G.; Dubrovinsky, L.S. On the compressibility of ferrite spinels: a high-pressure X-ray diffraction study of MFe_2O_4 (M = Mg, Co, Zn). *High Pressure Res.* **2009**, *29*, 764–779. [CrossRef]
26. Nakagiri, N.; Manghnani, M.H.; Ming, L.C.; Kimura, S. Crystal structure of magnetite under pressure. *Phys. Chem. Miner.* **1986**, *13*, 238–244. [CrossRef]
27. Mao, H.K.; Xu, J.; Bell, M. Calibration of the ruby pressure gauge to 800 kbar under quasi-hydrostatic conditions. *J. Geophys. Res.* **1986**, *91*, 4673–4676. [CrossRef]
28. Zhao, Y.S.; Lawson, A.C.; Zhang, J.Z.; Bennett, B.I.; Von Dreele, R.B. Thermoelastic equation of state of molybdenum. *Phys. Rev. B* **2000**, *62*, 8766. [CrossRef]
29. Angel, R.J.; Allan, D.R.; Miletich, R.; Finger, L.W. The use of quartz as an internal pressure standard in high-pressure crystallography. *J. Appl. Crystallogr.* **1997**, *30*, 461–466. [CrossRef]
30. Liu, X.; He, Q.; Deng, L.; Zhai, S.; Hu, X.; Li, B.; Zhang, L.; Chen, Z.; Liu, Q. Equation of state of CAS phase to pressure of the uppermost lower mantle at ambient temperature. *Sci. Chin. Earth Sci.* **2011**, *54*, 1394–1399. [CrossRef]